AC Microgrid Modeling and Adaptive Control Using Biomimetic Valence Learning: An AI-Based Approach

1st Abd Alelah Derbas
Department of Computer Science
The Arctic University of Norway, UiT
Tromø, Norway
abd.a.derbas@uit.no

2nd Chiara Bordin
Department of Computer Science
The Arctic University of Norway, UiT
Tromø, Norway
chiara.bordin@uit.no

3rd Sambeet Mishra
Department of Electrical, IT and Cybernetics
University of South Eastern Norway (USN)
Porsgrunn, Norway
sambeet.mishra@usn.no

4rd Mohsen Hamzeh
The School of Electrical and Computer Engineering
College of Engineering
University of Tehran (UT)
mohsenhamzeh@ ut.ac.ir

5th Frede Blaabjerg
Department of Energy
Aalborg University
Aalborg, Denmark
fbl@energy.aau.dk

***Abstract*—AC microgrids play a crucial role in integrating distributed energy resources and facilitating localized power management in contemporary power networks. Nevertheless, conventional droop control methods in these microgrids have constraints in guaranteeing precise power distribution, stability of voltage/frequency, and flexibility in response to changing operating conditions. This study introduces an approach, with adaptive droop control using Biomimetic Valence Learning (BVLAC). Inspired by the emotional and rational decision-making processes within the brain, BVLAC dynamically adjusts droop coefficients, optimizing power sharing and transient response in microgrid operation. Simulations were conducted using SIMULINK/MATLAB and the results showcase the superiority of the proposed BVLAC approach in achieving precise power-sharing, maintaining voltage and frequency stability, and improving the control performance of microgrids, under varying load conditions. This work advances the field of microgrid control by offering a robust, AI-inspired solution for the challenges faced by conventional droop control techniques.**

***Index Terms*—Artificial intelligent control, Biomimetic Valence Learning, Adaptive droop control**

I. Introduction

The growing incorporation of Distributed Energy Resources (DERs), such as solar and wind power, offers promising prospects for contemporary power networks. These DERs have the potential to strengthen the ability to recover quickly from disruptions, increase the effectiveness, and promote energy markets that are focused on specific local areas [1]–[3]. AC microgrids, also known as ACMGs, provide a flexible framework for effectively managing these resources. However, a primary obstacle persists: how to guarantee consistent and dependable power distribution in the case of the inherent unpredictability of renewable energy production and also changing electricity use [4]. To fully use the advantages of ACMGs, it is crucial to prioritize the creation and execution of efficient control methods [5] and advanced control approaches are necessary to enable effective and robust power management inside autonomous ACMGs. Traditional droop control has become a widely adopted method to achieve decentralized control in ACMGs. This approach mimics the behavior of synchronous generators, where active power-frequency and reactive power-voltage relationships govern the power-sharing among DERs [6]–[8]. However, conventional droop control has several limitations:

i Inaccurate power-sharing: Load changes and variations in DER output can lead to deviations from the proportional power-sharing and potentially overloading certain DERs [9].

ii Susceptibility to instability: Disturbances, rapid load variations, and line impedance mismatches can destabilize an ACMG operating under conventional droop control, leading to voltage and frequency fluctuations that exceed acceptable limits [10].

iii Sensitivity to parameter tuning: Fixed droop coefficients may not be optimal across diverse operating conditions. Manual tuning is complex and may not guarantee the best performance in dynamic scenarios [11].

In order to address these constraints, much study have been dedicated to the development of adaptive droop control strategies [12]–[14]. These techniques dynamically modify the droop coefficients in real time, optimizing the ACMG's response to various operating conditions. Ref. [12] streamlined AC-DC coupled droop control for VSC-based DC microgrids, removing the need for additional outer loops and boosting the bus voltage dynamics. Addressing stability concerns, [13] introduced a robust H_∞ multivariable stabilizer approach for

This work is funded by the Aurora Research Center

autonomous AC microgrids, improving the transient power sharing performance. Furthermore, in [14] a particle swarm optimization (PSO) method is used to fine-tune the droop control parameters, and the voltage deviation and power allocation accuracy are addressed.

Existing adaptive schemes improve the performance, yet often rely on system models, complex calculations, or manual tuning, hindering a widespread practical implementation [15]–[17]. Artificial intelligence (AI) has revolutionized various engineering domains and holds considerable promise in the field of power system control [18], [19]. AI techniques offer self-learning, data-driven approaches that can adapt to the complexities of ACMGs without requiring explicit system models. This enables enhanced power-sharing accuracy, improved transient response, and the potential for self-optimizing behavior [20]. Biomimetic Valence Learning (BVLAC) emerges as a novel AI-inspired approach, drawing insights from the biological learning mechanisms to steer optimization processes. BVLAC incorporates elements analogous to the brain's emotional regulation (amygdala), decision-making (prefrontal cortex), and information processing (sensory areas) [21]. This unique approach is here, presented for the first time to overcome the limitations of existing adaptive droop mechanisms, enabling a new generation of intelligent, robust, and self-tuning ACMG controllers. This paper presents a BVLAC as a new AI-based approach that is inspired by how living things learn. Its purpose is to assist in the development of self-tuning droop control. An intelligent adaptive droop control strategy is presented based on the principles of Biomimetic Valence Learning.

II. AC Microgrid Modeling

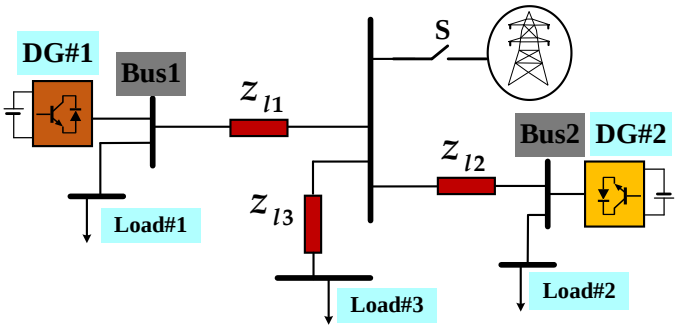

Fig. 1: Single-line diagram of the ACMG with two VSC based DG units and different loads, operating in islanded mode.

TABLE I: Parameters of ACMG

Parameter	Value	Parameter	Value
r_f , L_f, C_f	0.1 Ω, 4.3 mH, 15 μF	T_S	20 μSec
S_{L1}, S_{L2}, S_{L3}	0.8, 1.5, 1.28 kVA	V_{ref}	400 V
r_{l1}, r_{l2}, r_{l3}	2.8, 2, 1.1 mΩ	f_{ref}	50 Hz
L_{l1}, L_{l2}, L_{l3}	0.44, 0.32, 0.17 mH		

The layout depicted in Figure 1 portrays the configuration of the ACMG, featuring two Distributed Generation (DG) units operating as Voltage Source Converters (VSCs). These units have the responsibility of supplying power to both adjacent and remote loads. The ACMG functions independently in island mode. The decentralized control system, depicted in Figure 2, is installed in each DG unit to oversee the microgrid regulation. An LC filter with three phases is installed to

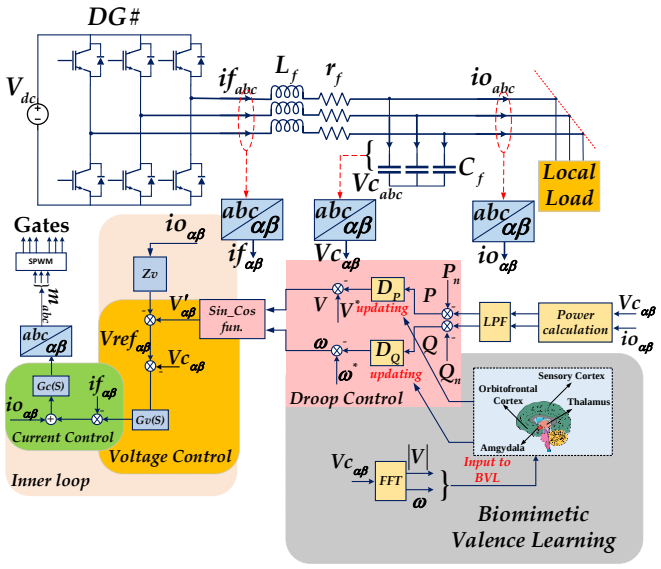

Fig. 2: Block diagram of the proposed control system for the ACMG, including droop control (outer loop) and voltage/current control (inner loops).

eliminate undesirable harmonics from the output voltage and current, while being linked to a load. The filter's dynamic model, as depicted in the $\alpha-\beta$ frame, is as follows:

$$L_f \frac{dif}{dt} = v_i - vc - i_f \cdot r_f$$
$$C_f \frac{dvc}{dt} = i_f - io \tag{1}$$

The filter comprises of two primary elements: the inductor (L_f) and the capacitor (C_f). The parameters of utmost importance are the input voltage (v_i) and the output current (i_o). The input voltage v_i is linked to both the dc-link voltage V_{dc} and the switching state vector.

In order to get the ability to regulate load voltages in the presence of disturbances, we convert the dynamic model into the stationary $\alpha-\beta$ frame by using the Clarke transformation $\mathbf{T}$. The system of equations can be represented as:

$$\dot{\mathbf{X}} = \mathbf{AX} + \mathbf{BU} + \mathbf{ED}, \qquad \mathbf{Y} = \mathbf{CX} \tag{2}$$

The equation employs matrices to symbolize various components of the system: $\mathbf{X}$ denotes state variables, $\mathbf{U}$ represents inputs, $\mathbf{D}$ signifies disturbances and $\mathbf{Y}$ stands for outputs.

The output voltage in the $\alpha-\beta$ frame is ultimately represented in the Laplace domain.

$$V_{c_{\alpha\beta}}(s) = M_{(2\times2)}(s)V_{i_{\alpha\beta}}(s) - N_{(2\times2)}(s)I_{o_{\alpha\beta}}(s) \tag{3}$$

The matrices $M_{(2\times2)}(s)$ and $N_{(2\times2)}(s)$ represent the decoupled dynamics of the system.

A. Voltage Control

The control system places the primary control at the forefront, structured to integrate droop control as the outer loop and voltage control as the inner loop. Its function is to control voltage and frequency at a local level during island mode operation. The primary control establishes the foundation for crucial control loops, such as the inner current and voltage loops, which are known as zero-level control. Here, the current control utilizes a PI controller with parameters Kc_p and Kc_i, which are adjusted to ensure internal stability. Meanwhile, the Proportional Resonant (PR) controller is responsible for regulating voltage, ensuring accurate tracking of the sinusoidal current reference signal in steady-state conditions.

When adjusting the parameters of (PR) and (PI) controllers, it is crucial to carefully evaluate the pulse width modulation (PWM) and calculation delay. Moreover, it is important to guarantee that the bandwidth of inner loops surpasses that of outer loops to avoid negative interactions. The voltage control system uses state feedback of i_f to improve the dynamic performance of the inner control loop and includes a feed-forward i_o to decrease dependence on the output load. Consequently, the first loop, which regulates the voltage of the capacitor, supplies reference signals to the current control loop. Nevertheless, conventional control systems have difficulties in rapidly adjusting to suddenly dynamic changes. To address problems such as steady-state error occurring at the fundamental frequency and successfully eliminate higher-order harmonics, the voltage control loop includes a proportional resonance control loop that comprises resonant filters. Then the transfer function of the PR controller can be represented as:

$$G_v(s) = K_P + \Sigma_{h=2n+1}^{\infty} \frac{K_h s}{s^2 + 2h\omega_c s + \omega_h^2} \quad n = 0, 1, 2, 3, ...\infty \tag{4}$$

Here, K_P and K_h denote the proportional and integral harmonic gains, respectively.

B. Droop Control

Conceptually, the VSC can be seen as voltage source with voltage amplitude (V_i) and power angle (δ_i). Considering the terminal bus voltage of $V_{\mathrm{g}}\angle 0$ and a connection line impedance of $z\angle\theta$, the exchange of apparent power can be expressed as follows:

$$S = V_{\mathrm{g}} I^* = \frac{V_{\mathrm{g}} V_i \angle\theta - \delta_i}{z} - \frac{V_{\mathrm{g}}^2 \angle\theta}{z} \tag{5}$$

then, the active and reactive power can be calculated as follows:

$$\begin{cases} P = \frac{V_{\mathrm{g}} V_i}{z} \cos(\theta - \delta) - \frac{V_{\mathrm{g}}^2}{z} \cos(\theta) \\ Q = \frac{V_{\mathrm{g}} V_i}{z} \sin(\theta - \delta) - \frac{V_{\mathrm{g}}^2}{z} \sin(\theta). \end{cases} \tag{6}$$

The transfer of active and reactive power in the VSC system is influenced by both the voltage magnitudes and the phase angle difference (δ) between the VSC and the AC bus. To simplify analysis, the concept of virtual impedance is employed. This approach ensures that the VSC perceives a well-defined output impedance, either purely inductive or purely resistive. Consequently, for inductive virtual impedance, the phase angle is typically assumed to be $\theta = 0^\circ$, while for resistive virtual impedance, $\theta = 90^\circ$ is used. Resistive virtual impedance is generally preferred due to its inherent characteristic of being independent of frequency variations and non-linear load effects. Furthermore, when the phase angle difference between the VSC voltage and the AC bus voltage is minimal, the cosine of δ (cosδ) can be approximated to 1, and the sine of δ (sinδ) can be approximated to δ itself. Under these assumptions, the droop control characteristic can be expressed as:

$$\begin{cases} \omega = \omega^* - D_Q Q \\ V = V^* - D_P P \end{cases} \tag{7}$$

where ω^* and V^* represent the reference frequency and amplitude for the voltage. D_Q and D_P are the droop coefficients.

The value of D_Q and D_P coefficients depend on the maximum allowable deviation of voltage and frequency. Usually, for a microgrid with N DGs and N resistive output impedances. these coefficients can be determined as a proportional expression with the rated power of each DG.

$$\begin{cases} D_{p_1} P_1 = D_{p_2} P_2 = \cdots = D_{p_i} P_i = \cdots D_{p_N} P_N = \Delta V_{\max} \\ D_{Q_1} Q_1 = D_{Q_2} Q_2 = \cdots = D_{Q_i} Q_i = \cdots D_{Q_N} Q_N = \Delta\omega_{\max} \end{cases} \tag{8}$$

P_i and Q_i, $i = 1, 2, ...N$ represent the nominal active and reactive power output of the ith DG, respectively. Similarly, $\Delta\omega_{\max}$ and $\Delta V_{\max}$ denote the maximum permissible deviations of the frequency and voltage, respectively.

The conventional techniques employed for adjusting droop coefficients present practical challenges, frequently requiring meticulous manual calibration endeavors. Nevertheless, AI methodologies emerge as promising alternatives for automating this intricate process. Furthermore, the integration of Biomimetic Valence learning (BVL) into these methodologies introduces a novel approach by assimilating emotional responses to steer the optimization process. This innovative approach is elaborated upon in the subsequent subsection.

III. Biomimetic Valence Learning for Adaptive Control (BVLAC)

BVLAC is a groundbreaking control framework. Unlike the traditional systems, it does not just work – it actively learns and adapts as the system itself changes. This adaptability is critical, and putting BVLAC at the forefront of research in various engineering fields. flexibility makes it to handle even the most complex and unpredictable scenarios. And its design is inspired the brain's complex processing mechanisms: BVLAC's design mimics of brain's elements: the amygdala (for affect regulation), the prefrontal cortex (for higher-order decision-making), sensory areas (for processing information), and the thalamus (for integrating that information). **Operational Framework** BVLAC's control process centers on the dynamic interaction between sensory data (X_i) and an

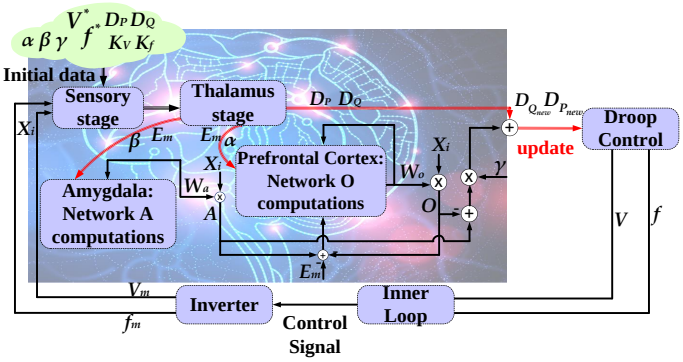

Fig. 3: Schematic representation of BVLAC and droop control interaction for adaptive D_p and D_q.

affective signal (E_m). Sensory information is first preprocessed and then transmitted to the system's equivalents of the amygdala and prefrontal cortex. The final control output, $u(t)$, is calculated as the difference between the outputs of Networks A and O:

$$u(t) = A(t) - O(t) \tag{9}$$

Network A: Excitatory Pathway Network A mimics a neural excitation pathway. It processes the sensory input (X_i) along with a weight parameter ($W_a(t)$) that continuously adapts over time:

$$A(t) = X_i(t) * W_a(t) \tag{10}$$

$W_a(t)$ is remarkably adaptable. Its learning mechanism is quite complex, driven by a weight adjustment function we call $\delta w_a(\tau)$. This function, along with the initial value $W_a(0)$, determines how quickly the weight can change over time.

$$W_a(t) = \int_0^t \delta w_a(\tau) d\tau + W_a(0) \tag{11}$$

$$\delta w_a(t) = \alpha * X_i(t) * [max(0, E_m(t) - A(t) - A_{\text{ref}}(t))] \tag{12}$$

$$A_{\text{ref}}(t) = \max[X_i] * W_{\text{ref}}(t) \tag{13}$$

Network O: Inhibitory Pathway Network O, serving a complementary inhibitory role, takes in sensory input (X_i), the affective signal (E_m), and the previous control output ($u(t-1)$). Its output is calculated as:

$$O(t) = X_i(t) * W_o(t) \tag{14}$$

Similar to Network A, the weight parameter $W_o(t)$ adapts over time. Its learning rule incorporates a factor (β) to adjust the strength of the inhibitory effect:

$$W_o(t) = \int_0^t \delta w_o(\tau) d\tau + W_o(0) \tag{15}$$

$$\delta w_o(t) = \beta * X_i(t) * [A(t) - O(t) - E_m(t)] \tag{16}$$

Integrated Control Dynamics The complete formulation for the BVLAC control output ($u(t)$), including initial conditions ($W_a(0) = W_o(0) = W_{\text{ref}}(0) = 0$), demonstrates the continuous adaptation of Networks A and O. This integrated control scheme is what enables the system to respond robustly to ever-changing system dynamics.

Algorithm 1 Adaptive Droop Coefficients Tuning Algorithm with BVLAC (see Fig. 3)

Input: V_{m}, f_{m}
Given: V^*, f^*, K_v, K_f, D_P, D_Q, α, β, γ
Output: $D_{P_{\text{new}}}$, $D_{Q_{\text{new}}}$
$\Delta V = V^* - V_{\text{m}}$
$\Delta f = f^* - f_{\text{m}}$
if $|\Delta V| \leq e_v$ **and** $|\Delta f| \leq e_f$ **then**
  return Dp, Dq
end if
$E_m = [K_v, K_f]^T \cdot [(\Delta V), (\Delta f)]$
$A = [V_{\text{m}}, f_{\text{m}}]^T \cdot [W_{va}, W_{fa}]$
$A_{\text{ref}} = [\max(V_{\text{m}}), \max(f_{\text{m}})] \cdot 0.5$
Solve (12) $\Rightarrow$ δW_{va}, δW_{fa}
$W_a \leftarrow W_a + \delta W_a$
Solve (14) $\Rightarrow$ δO_{va}, δO_{fa}
Solve (16) $\Rightarrow$ δW_{vo}, δW_{fo}
$W_o \leftarrow W_o + \delta W_o$
$[D_{P_{\text{new}}}, D_{Q_{\text{new}}}]^T = [D_P, D_Q]^T + \gamma \cdot [V_{\text{m}}, f_{\text{m}}]^T \cdot W_a - [V_{\text{m}}, f_{\text{m}}]^T \cdot W_o)$
return $D_{P_{\text{new}}}$, $D_{Q_{\text{new}}}$

where: V_{m} and f_{m} are the measured voltage and frequency from the microgrid, V^* and f^* are the desired voltage and frequency setpoints, D_P and D_Q are the current droop coefficients for active power and reactive power, e_v and e_f are the acceptable voltage and frequency deviation tolerances, α controls how quickly the learning rate adapts based on error size, β is the smoothing factor applied to updates, promoting smoother convergence, γ is a convergence smoothing factor applied to updates of the droop coefficients. It promotes smoother and more gradual adjustments. $D_{P_{\text{new}}}$ and $D_{Q_{\text{new}}}$ are the updated droop coefficients for active power and reactive power. K_v and K_f are constants to adjust how strongly the voltage and frequency errors impact the affective signal. The BVLAC and droop control interaction for adaptive D_p and D_q is shown in Fig. 3

IV. Simulation and Results

To thoroughly assess the proposed BVLAC method, simulations are carried out through MATLAB SimPowerSystems. The purpose of these simulations is to assess the effectiveness of the proposed control in an ACMG consisting of two VSC-DGs, as shown in Figure 1. The system was set up with a standard voltage of 400V and a frequency of 50 Hz. The system parameters of the microgrid are shown in Table I.

A. Performance Assessment: Dynamic Load Changes

To assess the controller's ability to adapt to real-time changes, we conducted a simulation in which the distributed generators (DGs) encountered a sequence of load variations.

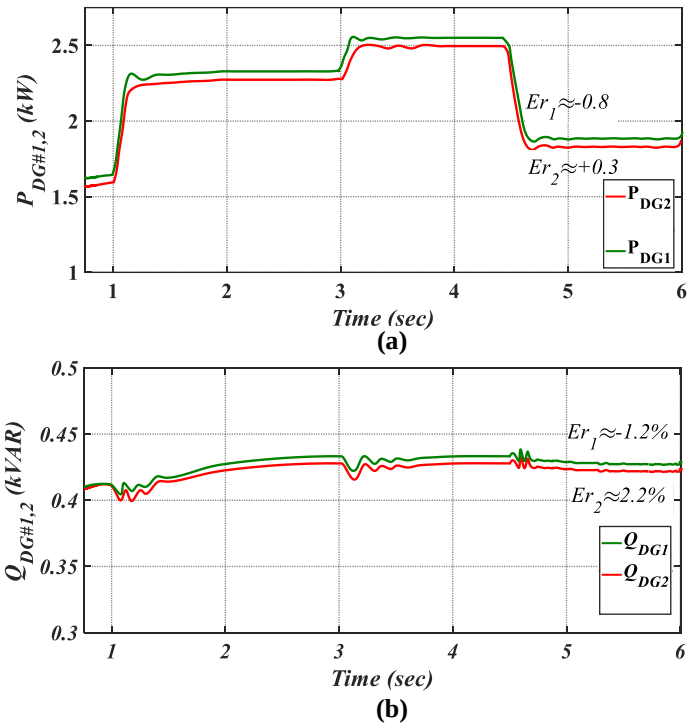

Fig. 4: Active (a) and Reactive (b) power sharing with proposed controller under different load variations.

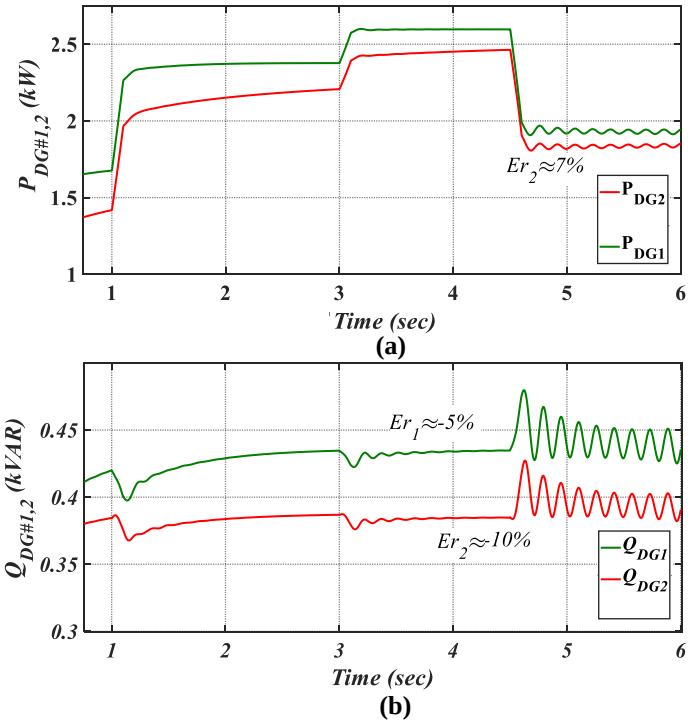

Fig. 5: Active (a) and Reactive (b) power sharing with conventional controller under different load variations.

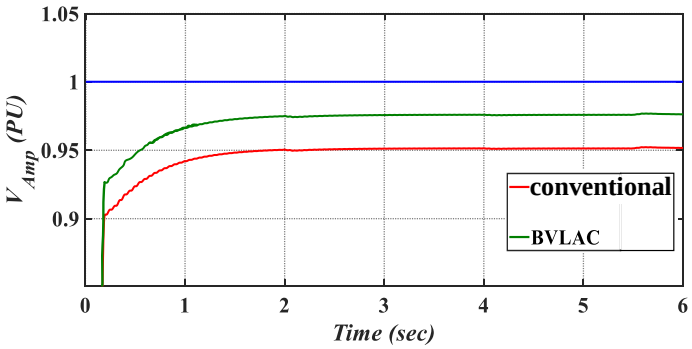

Fig. 6: Error of output voltage amplitude of DG#1 with conventional and BVLAC control.

Load #2 had a significant surge of 35%, followed by a subsequent lesser rise by 12%, and ultimately a severe decline by 35%. Fig. 4 and 5 depict the allocation of active and reactive power between DG #1 and #2 during the whole duration for both the proposed and conventional controls. The proposed controller effectively manages power via these changes, demonstrating its impressive ability to navigate changing system states. The active power sharing error was -0.8% for DG #1 and 0.3% for DG #2. The reactive power sharing error exhibited a modest increase in absolute by 1.2% for DG #1 and 2.2% for DG #2, while they remained within an acceptable range. The the conventional control shows the following errors -10% for DG #1 and 7% for DG #2 for the active power and -5% for DG #1 and -10% for DG #2 or the reactive power, under general, the controller effectively demonstrates its capacity to maintain constant voltage and frequency, and even mitigate harmonics under challenging conditions. This indicates a resilient architecture. Fig. 6 compares the error in output voltage amplitude of DG#1 under conventional droop control and the proposed BVLAC method. The conventional droop control exhibits a 5% error, while the BVLAC method reduces this error to approximately 2.5%. Similarly, Fig. 7 demonstrates the frequency regulation improvement with BVLAC. The conventional droop control results in a 0.3 Hz (0.6%) frequency error, whereas the BVLAC method significantly reduces this error to be less than 0.05 Hz (< 0.1%), due to the online tuning of the droop controller parameters according to the operation conditions, while in conventional droop controller the parameters designed according to the allowable limitations of droop voltage/ frequency.

V. Conclusion

This study indicates that Biomimetic Valence Learning (BVLAC) shows potential in addressing some of the drawbacks using droop control in AC microgrids. While traditional methods can struggle with power sharing, voltage/frequency stability, and adapting to changing conditions, the BVLAC approach offers a flexible and self-tuning way to tackle these issues. Drawing inspiration from how the brain blends emotion and logic BVLAC modifies the control parameters of the microgrid. Simulations have shown that BVLAC enhances

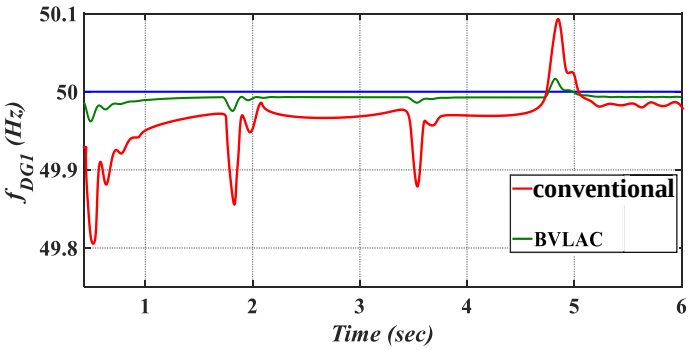

Fig. 7: Frequency variations of DG#1 with conventional and BVLAC control

power-sharing accuracy, improves the voltage and frequency regulation, and improves response times within the microgrid. Notably, it is better than the conventional control when dealing with varying load conditions. This research pushes forward the realm of microgrid control by introducing an AI-inspired approach. There is an opportunity to investigate how BVLAC could function in microgrids that incorporate a mix of energy sources and more intricate loads. It would also be intriguing to implement BLAC, within hierarchical control of microgrid system.

ACKNOWLEDGMENT

This research is supported by the UiT Aurora project MASCOT - Mathematical Structures in Computation.

REFERENCES

[1] H. Han, X. Hou, J. Yang, J. Wu, M. Su, and J. M. Guerrero, "Review of power sharing control strategies for islanding operation of ac microgrids," *IEEE Transactions on Smart Grid*, vol. 7, no. 1, pp. 200–215, 2016.

[2] S. Ahmad, M. Shafiullah, C. B. Ahmed, and M. Alowaifeer, "A review of microgrid energy management and control strategies," *IEEE Access*, vol. 11, pp. 21729–21757, 2023.

[3] A. A. Derbas and M. Hamzeh, "A new power sharing method for improving power management in dc microgrid with power electronic interfaced distributed generations," in *2019 27th Iranian Conference on Electrical Engineering (ICEE)*, pp. 624–629, 2019.

[4] A. Oshnoei, A. A. Derbas, S. Peyghami, and F. Blaabjerg, "Robust control of voltage source converters: A tube-based model predictive approach," *IEEE Transactions on Circuits and Systems II: Express Briefs*, vol. 70, no. 9, pp. 3464–3468, 2023.

[5] M. Roslan, M. Hannan, P. J. Ker, and M. Uddin, "Microgrid control methods toward achieving sustainable energy management," *Applied Energy*, vol. 240, pp. 583–607, 2019.

[6] J. M. Guerrero, J. C. Vasquez, J. Matas, L. G. de Vicuna, and M. Castilla, "Hierarchical control of droop-controlled ac and dc microgrids—a general approach toward standardization," *IEEE Transactions on Industrial Electronics*, vol. 58, no. 1, pp. 158–172, 2011.

[7] A. Vasilakis, I. Zafeiratou, D. T. Lagos, and N. D. Hatziargyriou, "The evolution of research in microgrids control," *IEEE Open Access Journal of Power and Energy*, vol. 7, pp. 331–343, 2020.

[8] A. A. Derbas, A. Oshnoei, M. Kheradmandi, and F. Blaabjerg, "Intelligent primary control of voltage source converters in ac microgrids," in *IECON 2022 – 48th Annual Conference of the IEEE Industrial Electronics Society*, pp. 1–6, 2022.

[9] F. Nejabatkhah and Y. W. Li, "Overview of power management strategies of hybrid ac/dc microgrid," *IEEE Transactions on Power Electronics*, vol. 30, no. 12, pp. 7072–7089, 2015.

[10] A. A. Eajal, A. H. Yazdavar, E. F. El-Saadany, and K. Ponnambalam, "On the loadability and voltage stability of islanded ac–dc hybrid microgrids during contingencies," *IEEE Systems Journal*, vol. 13, no. 4, pp. 4248–4259, 2019.

[11] Y. Liu, Z. Li, and J. Zhao, "Safety-constrained stagewise optimization of droop control parameters for isolated microgrids," *IEEE Transactions on Smart Grid*, vol. 15, no. 1, pp. 77–88, 2024.

[12] B. Zhang, F. Gao, Y. Zhang, D. Liu, and H. Tang, "An ac-dc coupled droop control strategy for vsc-based dc microgrids," *IEEE Transactions on Power Electronics*, vol. 37, no. 6, pp. 6568–6584, 2022.

[13] R. K. Sharma, S. Mishra, and D. Pullaguram, "A robust h_∞ multivariable stabilizer design for droop based autonomous ac microgrid," *IEEE Transactions on Power Systems*, vol. 35, no. 6, pp. 4369–4382, 2020.

[14] L. Zhang, H. Zheng, Q. Hu, B. Su, and L. Lyu, "An adaptive droop control strategy for islanded microgrid based on improved particle swarm optimization," *IEEE Access*, vol. 8, pp. 3579–3593, 2020.

[15] K. Lu, Z. Liu, H. Yu, C. L. P. Chen, and Y. Zhang, "Inverse optimal adaptive neural control for state-constrained nonlinear systems," *IEEE Transactions on Neural Networks and Learning Systems*, pp. 1–12, 2023.

[16] C. Yang, T. Zheng, M. Bu, P. Li, and J. M. Guerrero, "Distributed model-free adaptive control strategy for hybrid ac/dc microgrid with event-triggered mechanism," *IEEE Transactions on Industrial Electronics*, vol. 71, no. 8, pp. 9077–9086, 2024.

[17] A. A. Derbas, A. Oshnoei, M. A. Azzouz, A. S. A. Awad, F. Blaabjerg, and A. Anvari-Moghaddam, "Adaptive damping control to enhance small-signal stability of dc microgrids," *IEEE Journal of Emerging and Selected Topics in Power Electronics*, vol. 11, no. 3, pp. 2963–2978, 2023.

[18] Y. Zhou, R. Arghandeh, and C. J. Spanos, "Partial knowledge data-driven event detection for power distribution networks," *IEEE Transactions on Smart Grid*, vol. 9, no. 5, pp. 5152–5162, 2018.

[19] A. A. Derbas, C. Bordin, S. Mishra, M. Hamzeh, and F. Blaabjerg, "Ann-based real-time optimal voltage control in islanded ac microgrids," in *PEDG 2024 IEEE 15th International Symposium on Power Electronics for Distributed Generation Systems*, 2024.

[20] Z. Shi, W. Yao, Z. Li, L. Zeng, Y. Zhao, R. Zhang, Y. Tang, and J. Wen, "Artificial intelligence techniques for stability analysis and control in smart grids: Methodologies, applications, challenges and future directions," *Applied Energy*, vol. 278, p. 115733, 2020.

[21] E. H. Houssein, A. Hammad, and A. A. Ali, "Human emotion recognition from eeg-based brain–computer interface using machine learning: a comprehensive review," *Neural Computing and Applications*, vol. 34, no. 15, pp. 12527–12557, 2022.